Thermodynamic Profiling at the Alpine Venue of the 2010 Winter Olympics

Randolph Ware[1,2,3], Domenico Cimini[4], Graziano Giuliani[4], Edwin Campos[5], Jeos Oreamuno[1], Paul Joe[5], Stewart Cober[5], Steve Albers[6,7], Steven Koch[7], Ed Westwater[3]

[1]Radiometrics; [2]NCAR; [3]CIRES (Boulder, CO USA)
(ware@radiometrics.com, 303 539-2313 tel, 303 786-9343 fax)
[4]CETEMPS, University of L'Aquila, Italy; [5]Meteorological Research Division, Environment Canada
[6]CIRA, Ft. Collins, CO USA; [7]NOAA ESRL GSD, Boulder, CO USA

Abstract

Environment Canada operated a thermodynamic profiling radiometer providing continuous temperature, humidity and liquid soundings during the Alpine Venue of the 2010 Winter Olympic Games. Retrievals were obtained in real time via neural networks and in post-processing via one-dimensional variational analysis (1DVAR). Background error covariance matrices for 1DVAR were calculated using brightness temperature from radiometer observations and from forward-modeled radiosonde and grid point model analysis. All radiometer, radiosonde and analysis data including all weather (rain, sleet and snow) conditions were included. 1DVAR retrieval errors, determined by comparison with radiosonde temperature and humidity soundings, are 1.6 C and 0.6 g/m^3 rms or less from the surface to 10 km height. This error is smaller than the representativeness error assigned to radiosonde data when they are assimilated into numerical weather models. These results suggest that 1DVAR retrievals are ready for operational use in numerical weather modeling and prediction.

Introduction

Radiometer, radiosonde and LAPS (Local Analysis and Prediction) analysis grid point locations are shown in Figure 1. The Radiometrics MP-3000A thermodynamic profiling radiometer observes 35 microwave (and 1 infrared) channels. Radiosondes were launched from the valley floor, 117 m below the mountainside radiometer site.

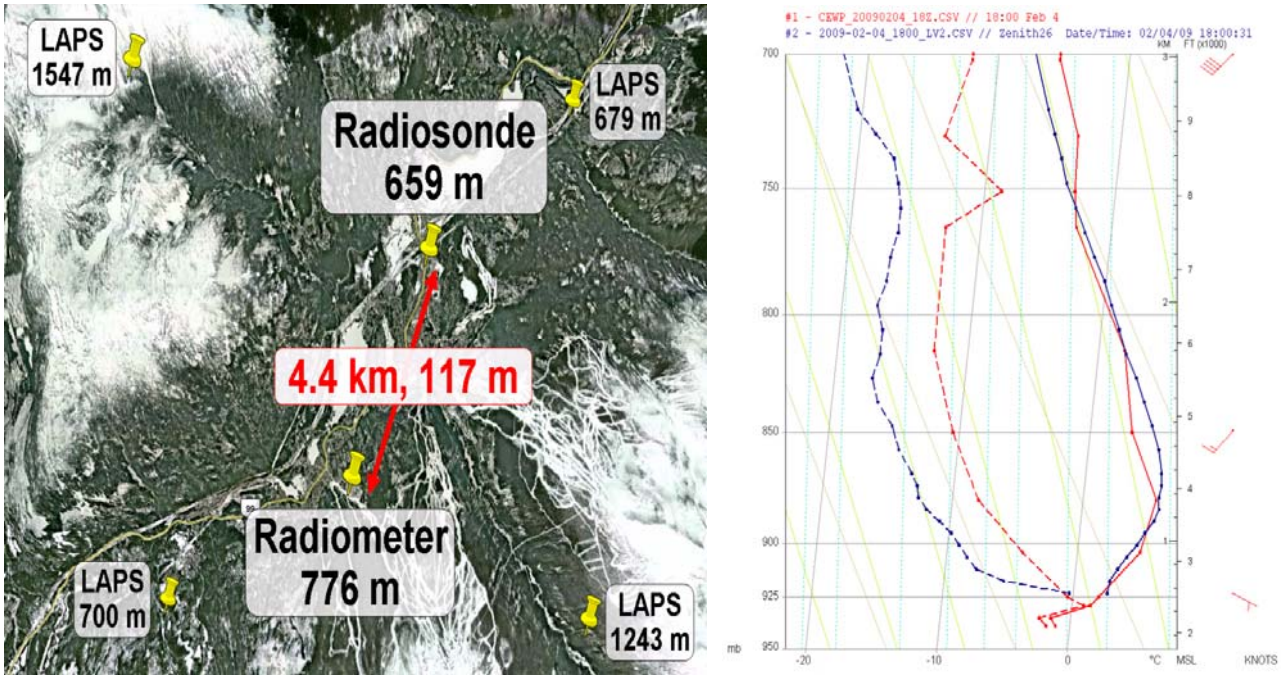

Figure 1. Radiometer, radiosonde and LAPS grid point locations in Whistler Valley (left); example radiometer (blue) and radiosonde (red) temperature and dewpoint soundings (right).

Also shown in Figure 1 are skew-T radiometer and radiosonde temperature and dewpoint soundings showing fog at the radiosonde site and clear conditions at the radiometer site. The temperature soundings show good agreement up to 10 km height, whereas dewpoint sounding agreement degrades with height (consistent with increasing separation during radiosonde ascent). The radiometer site and the radiosonde launch site are shown in Figure 2.

Figure 2. Meteorological sensors (radiometer second from left) on the mountainside at the base of the Creekside Gondola, and the radiosonde launch site in the Whistler valley.

Observations

Surface and cloud base temperatures measured by the radiometer are shown in Figure 3. When cloud base and surface temperature are similar, low clouds are present; cloud base temperatures near 180 K indicate clear conditions. In general, it was cloudy 12-17 and 23-26 Feb and clear 18-22 Feb.

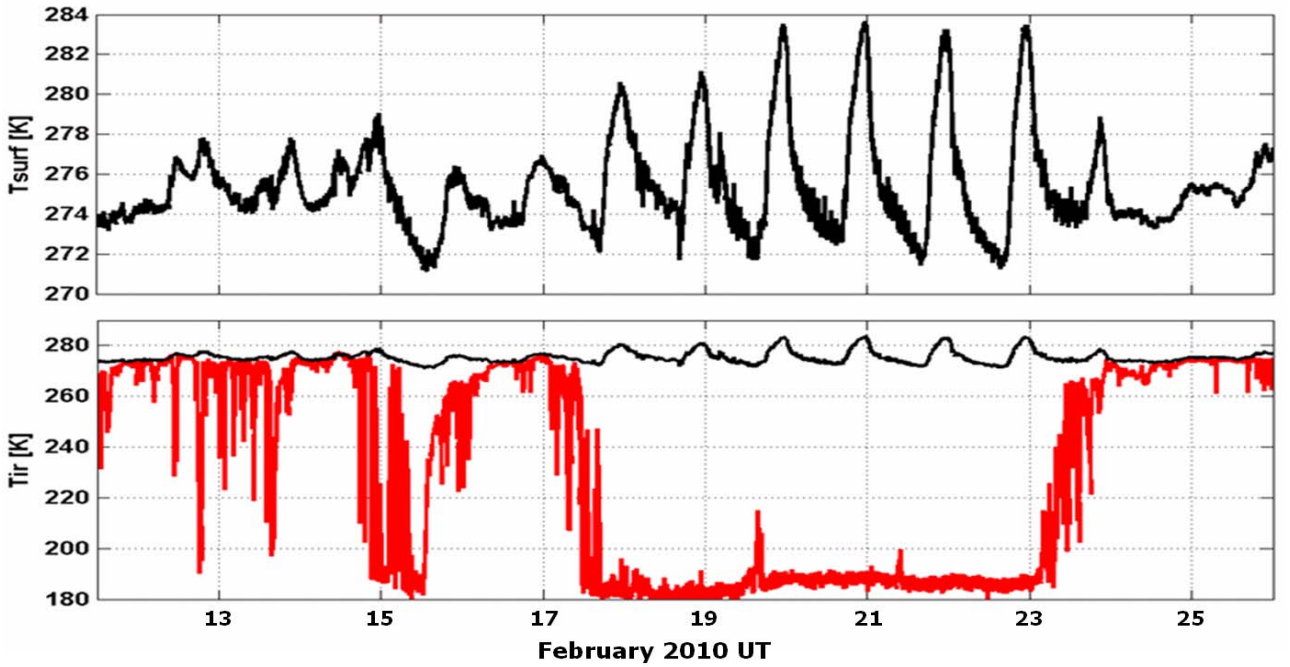

Figure 3. Surface temperature (black) and cloud base temperature (red).

Brightness temperatures observed by radiometer and forward modeled from LAPS analysis and radiosondes are shown in Figure 4.

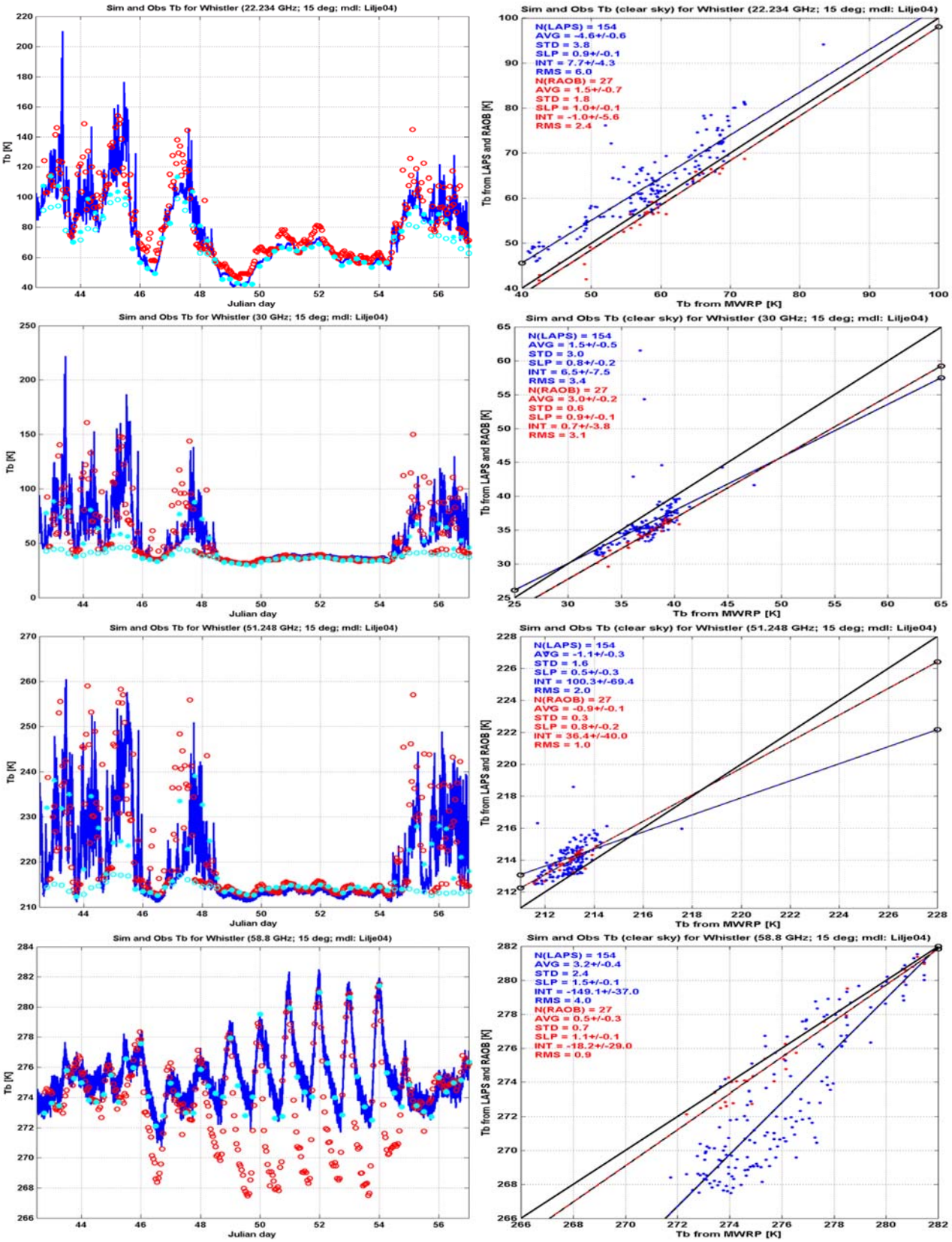

Figure 4. Radiometer (blue), analysis (red) and radiosonde (clear: solid cyan; cloudy: open cyan) brightness temperature time series (left) and scatter plots (right – clear only) at 22, 30, 51 and 59 GHz (top to bottom).

Radiometer, radiosonde and analysis brightness temperatures are in reasonably good agreement, except at 58.8 GHz, where the analysis is up to 7 C colder after sunset during clear conditions. Reduction in model nighttime boundary layer height is expected to improve agreement at 58.8 GHz (and nearby frequencies).

Retrievals

Radiometer (neural network) and radiosonde temperature, relative humidity and liquid water profiles for the 2 week Winter Olympic time period are shown in Figure 5.

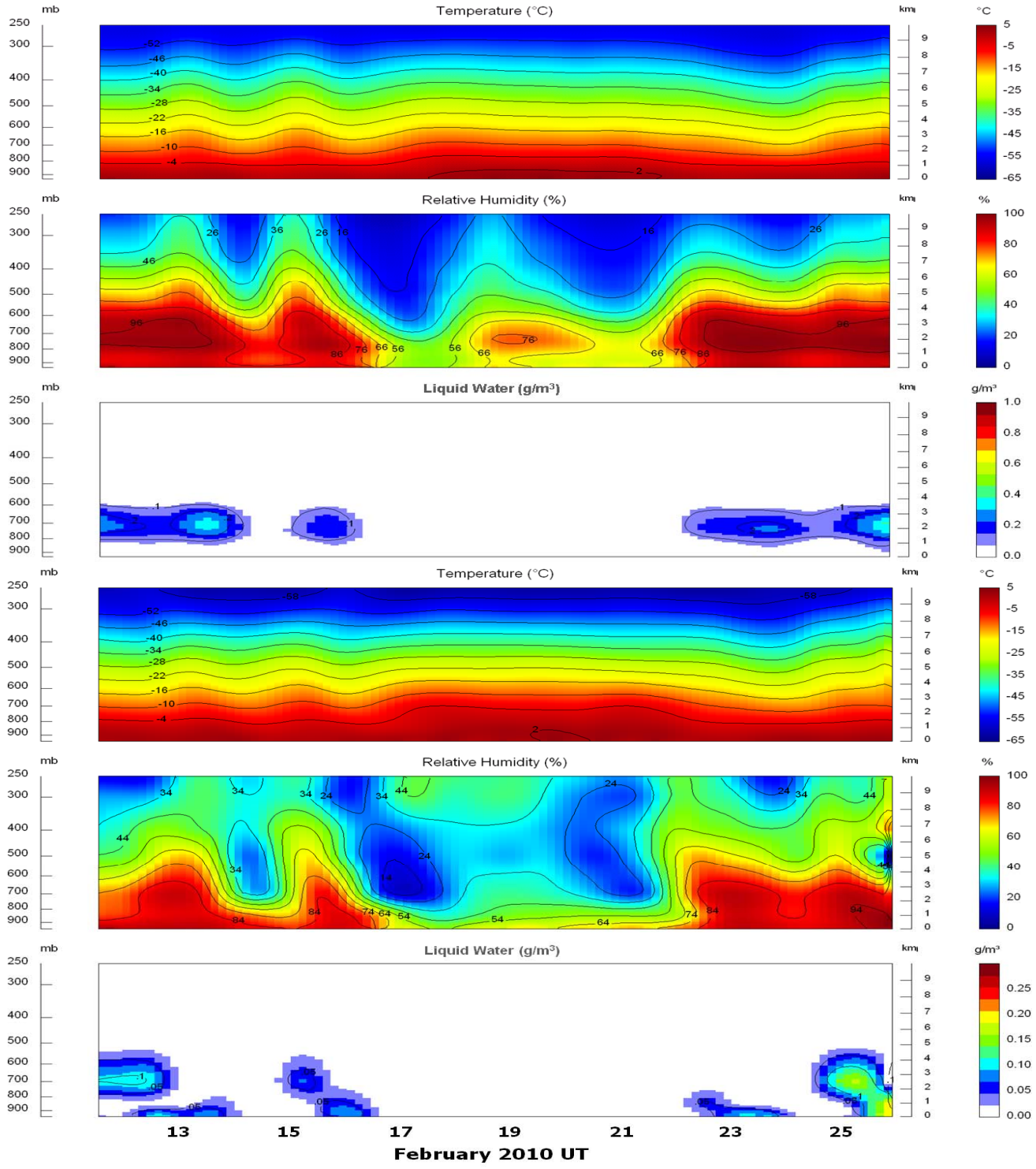

Figure 5. Radiometer off-zenith neural network (top) and radiosonde (bottom) temperature, humidity and liquid water profiles during the Winter Olympics.

Radiometer and radiosonde temperature and humidity profiles (Figure 5) are similar during cloudy, clear and precipitating (rain, sleet and snow) conditions. However, the liquid profiles show significant differences. Maximum radiometer liquid is 1 g/m^3, whereas maximum liquid estimated from radiosondes (Decker et al., 1978) are a factor of three

smaller (0.3 g/m^3). Also, the radiosonde, located in the valley, shows fog, whereas the mountainside radiometer does not.

Covariance

Background error covariance matrices computed from simultaneous radiosonde, analysis and radiometer brightness temperatures are shown in Figure 6.

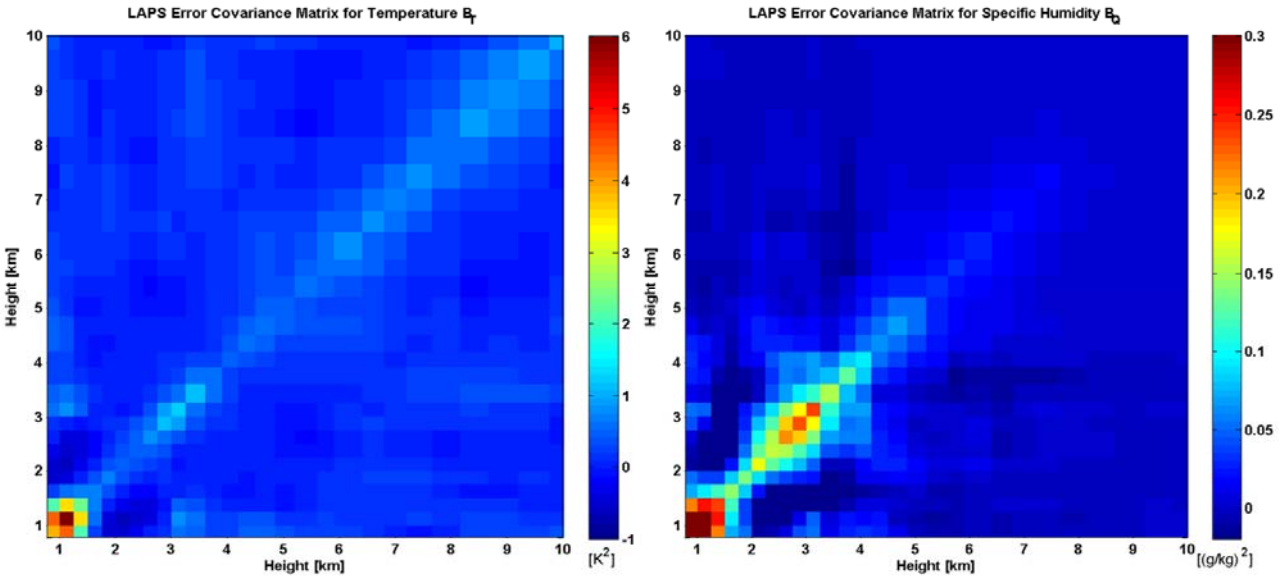

Figure 6. Temperature (left) and vapor density (right) background error covariance matrices.

Statistical comparisons of neural network and 1DVAR retrievals with radiosondes are shown in Figure 7.

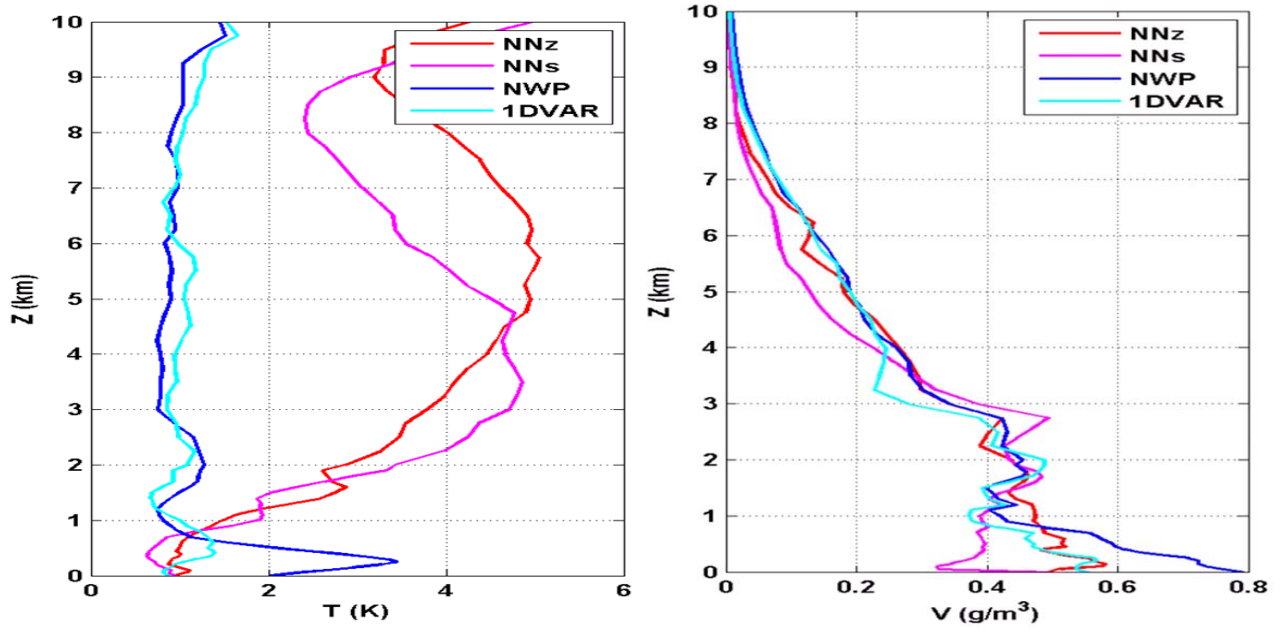

Figure 7. Zenith (NNz) and off-zenith (NNs) neural network, analysis (NWP) and 1DVAR temperature (left) and vapor density (right) statistical comparisons (rms) with radiosondes.

The LAPS analysis (NWP) temperature accuracy is good at heights down to 800 m, and the neural network retrieval accuracy is good up to 800 m. Above ~1 km neural network temperature retrieval errors are roughly three times larger than long-term statistical errors reported during non-precipitating conditions (Güldner and Spänkuch, 2001). We attribute the larger error for zenith (NNz) retrievals to rain, sleet and snow accumulation on top of the radiometer radome, and for off-zenith (NNs) retrievals to leveling error (small leveling

error can generate several K brightness temperature error). In general, 1DVAR retrievals at all heights provide better accuracy than the representativeness error (Kistler et al., 2001; Knupp et al., 2009) universally assigned to radiosonde data when they are assimilated into numerical weather models.

Results

Observed (radiometer) and forward modeled (radiosonde and analysis) brightness temperature time series and scatter plot comparisons during clear sky show similar trends. Clear sky radiosonde (RAOB) and analysis (LAPS) brightness temperature comparisons with radiometer observations show the following:

1) RAOB 22 and 30 GHz channels show 1.5 to 3.0 K bias. This may be caused by one or more of the following: (a) radiosonde dry-bias, (b) water vapor absorption model uncertainty, (c) radiometer calibration bias, and (d) radiometer leveling error.
2) RAOB 51 and 59 GHz channels agree very well (within the expected accuracy) except for 1-2 K bias in the 51.1-52.8 GHz channels. This may be caused by radiometer leveling error (0.1 deg leveling error may cause several K brightness temperature error).
3) LAPS 22 and 30 GHz channels show 3 to 4 K average bias and upper channels show bias similar to RAOB. This is consistent with LAPS moisture overestimation in the upper troposphere-lower stratosphere for the lower channels and by (1a-d) above for the upper channels.
4) LAPS 51 and 59 GHz channels show significantly different slope for most channels. This is consistent with a ~5 K overestimation of the thermal diurnal cycle by LAPS.

Radiometer (neural network) and radiosonde temperature and humidity profiles show similar upper tropospheric temperature variations. Liquid profiles estimated from radiosondes show three times lower maximum liquid density compared to radiometer retrievals.

Conclusions

1DVAR methods can provide continuous temperature and humidity soundings for numerical weather modeling with accuracy equivalent to radiosondes. The method, demonstrated during all weather conditions (rain, sleet and snow) during the 2010 Winter Olympics, is quasi-operational (ready for operational forecasting).

References

Cimini, D., E. Westwater and A. Gasiewski, Temperature and humidity profiling in the Arctic using ground-based millimeter-wave radiometry and 1DVAR, **TGARS**, 2009.

Decker, M., E. Westwater and F. Guiraud, Experimental Evaluation of Ground-Based Microwave Sensing of Atmospheric Temperature and Water Vapor, **JAM**, 1978.

Kistler, R., E. Kalnay, W. Collins, S. Saha, G. White, J. Woolen, M. Chelliah, W. Ebiszusaki, M. Kanamitsu, V. Kousky, H. van den Dool, R. Jenne and M. Fiorino, The NCEP-NCAR 50 Year Reanalysis, **BAMS**, 2001.

Knupp, K., R. Ware, D. Cimini, F. Vandenberghe, J. Vivekanandan, E. Westwater and T. Coleman, Ground-Based Passive Microwave Profiling during Dynamic Weather Conditions, **JAOT**, 2009.

Güldner J., and D. Spänkuch, **Remote Sensing of the Thermodynamic State of the Atmospheric Boundary Layer by Ground-Based Microwave Radiometry**, **JAOT**, 2001.

Westwater, E., D. Cimini, M. Klein, V. Leuski, V. Mattioli, A. Gasiewski, S. Dowlatshahi, J. Liljegren, B. Lesht and J. Shaw, Microwave and Millimeter Wave Forward Modeling Results from the 2004 North Slope of Alaska Arctic Winter Radiometric Experiment, **ARM-STM**, 2005.